Hindawi
Advances in Mathematical Physics
Volume 2021, Article ID 9200267, 16 pages
https://doi.org/10.1155/2021/9200267

Research Article

Mean Deviation Coupling Control for Multimotor System via Global Fast Terminal Sliding Mode Control

Changlin Zhu, Qunzhang Tu, Chengming Jiang, Ming Pan, Hao Huang, and Zhiwen Tu

College of Field Engineering, Army Engineering University of PLA, Nanjing 21007, China

Correspondence should be addressed to Qunzhang Tu; tqzlhnj@126.com

Received 26 July 2021; Accepted 2 September 2021; Published 13 September 2021

Academic Editor: Leopoldo Greco

In view of the shortcomings of the existing multimotor synchronous control strategy, a new method of mean deviation coupling control for multimotor system via global fast terminal sliding mode control is proposed. Firstly, the mathematical model of permanent magnet synchronous motor (PMSM) under a d-q reference frame is established. Next, based on the deviation coupling control, the deviation is calculated by the average speed, and the structure of the deviation coupling control strategy is optimized. The speed controller of the multimotor system is designed based on the global fast terminal sliding mode control (GFTSMC) algorithm to improve the synchronization accuracy of the system. In addition, a load torque Luenberger observer is designed to observe the load in real time. Then, the stability analysis of the controller is carried out by using the Lyapunov function. Finally, a four-motor experimental platform is built to verify the effectiveness of the proposed control strategy.

1. Introduction

Permanent magnet synchronous motor is widely used in industrial production and electric vehicle because of its high-power density, simple structure, and high efficiency [1]. However, a single motor is difficult to meet the needs of high performance and high precision in many applications, so multi-motor drive system has become a research hotspot in recent years [2, 3]. Although the same speed signal is given to each motor, the output speed of each motor would be inconsistent due to the load interference in the working process, and the synchronization performance of the system would be affected. Therefore, multimotor synchronous control has become one of the key technologies of the multimotor drive system [4]. As early as last century, research on the synchronous control strategy of multimotors has been carried out by researchers. After decades of development, the master-slave control strategy, crosscoupling control strategy, adjacent crosscoupling control strategy, ring coupling control strategy, deviation coupling control strategy, virtual spindle synchronous control strategy, and so on have been proposed for the multimotor system [5–13].

In the master-slave control strategy, one motor is selected as the master motor, the other motor is the slave motor, and the output speed signal of the master motor is used as the input speed signal of the slave motor. The structure is simple [14]. When the master motor speed changes, the speed of the slave motor changes accordingly. But when the speed of one slave motor changes, the signal cannot be fed back to other motors, which causes the speed to be out of sync [15]. In the crosscoupling control strategy, the speed difference between the two motors is used as the compensation signal and fed back to the motor controller [16]. In order to improve the synchronization performance, fuzzy control algorithm, adaptive control-algorithm, neural network algorithm, and second-order sliding mode control algorithm are applied to the crosscoupling control strategy [17–21]. However, the crosscoupling control strategy is only suitable for the dual motor system. For this reason, Zhao et al. [9] proposed adjacent crosscoupling control. For any motor, only the speed of two motors adjacent to it is taken into account. But when the number of motors is greater than 3, there will always be a motor whose control is lagging behind [22].

The ring coupling control takes into account the error between the motor output speed and the given speed and the error between the adjacent motor speeds, so it can be applied to the multimotor system with more than three motors [11]. However, the speed difference feedback of adjacent motors in the ring coupling control is unidirectional. When the number of motors is large, the whole system has a large feedback delay, and its response speed needs to be improved. According to the relationship between the speed difference and the speed deviation of each motor, the deviation coupling control compensates the speed of each motor to achieve the advantages of good synchronization performance and fast response speed [4]. But the structure of the system is complex, and the calculation of the system is very large [23]. The synchronous control of virtual spindle is evolved from mechanical axis, and the link of each unit is no longer constrained by distance and has larger output power. However, there is an essential defect in its structure; there is a steady-state error between the output of the motor and the reference of the output of the virtual axis. When the system is started or stopped or when a single motor is disturbed, there would be a phenomenon of misalignment between the axes [24].

The control accuracy of multimotor synchronous control strategy is closely related to its control algorithm. In this regard, many control algorithms have been proposed, such as proportional integral derivative (PID) control, sliding mode control (SMC), fuzzy control, and neural network control [25–28]. Because PMSM is a nonlinear, multivariable, and strongly coupled control object [29] and sliding mode control has the advantages of simple algorithm and insensitive to parameter changes and disturbances, so sliding mode control algorithm is very suitable for multimotor synchronous control [30]. However, because of the discontinuous switching characteristics of conventional SMC, the chattering phenomenon of increasing system energy consumption and reducing system stability is caused. In order to suppress the chattering phenomenon, the concepts of "quasisliding mode" and "boundary layer" were introduced into the design of SMC [31], and the chattering phenomenon is suppressed effectively. However, the control effect and inhibition effect cannot be optimal at the same time because of the selection of boundary layer thickness. Gao introduced the concept of reaching law into the design of sliding mode variable structure control [32] and proposed a chattering elimination method, which ensures the dynamic quality of sliding mode dynamic arrival process by adjusting the parameters of reaching law. But larger parameters will cause chattering. Sun et al. [33] proposed a fuzzy sliding mode control strategy by combining fuzzy control rules with sliding mode variable structure control to achieve the purpose of suppressing chattering.

Although the above methods can suppress the chattering to a certain extent, the chattering problem cannot be solved fundamentally, which is rooted in the switching term in the conventional SMC. One of the methods to solve the chattering problem is to design terminal sliding mode control (TSMC) strategy by using nonlinear function instead of switching term in SMC [34]. Zhuang et al. [35] designed a terminal sliding surface for high-order nonlinear systems to overcome the disadvantage of discontinuous derivatives of conventional SMC sliding surface. But the common terminal sliding mode controller has singularity problem. In order to solve the singular problem in the ordinary TSMC, Feng et al. [36] put forward a nonsingular terminal sliding mode control strategy, which solves the singular problem better. For nonlinear systems, Liu et al. [37] proposed GFTSMC, which avoids the singularity problem, and the response speed of the system is improved, and the chattering in the SMC is eliminated effectively.

Aiming at the shortcomings of the existing multimotor synchronization control strategy, mean deviation coupling control for multimotor system via global fast terminal sliding mode control is proposed in this paper, and the advantages of good synchronization performance and fast response speed of deviation coupling control is retained. The average speed is used to replace the speed difference between each motor, which simplifies the structure of deviation coupling control strategy and reduces the calculation of the system. The GFTSMC algorithm is used to solve the chattering problem in sliding mode control and to improve the response speed and control accuracy of the system. In addition, to solve the problem of unmeasurable load torque, a load torque Luenberger observer is designed to estimate the load of the motor in real time and feedback it to the controller. The remaining chapters of this paper are arranged as follows: in Section 2, the mathematical model of PMSM is established. The mean deviation coupling controller for multimotor system via global fast terminal sliding mode control and load torque Luenberger observer is designed in Section 3. In Section 4, the stability of the controller is analyzed by using the Lyapunov function, and the four-motor system platform is built to verify the effectiveness of the mean deviation coupling control strategy for multimotor system via global fast terminal sliding mode control in Section 5, and the conclusion of this paper is given in Section 6.

2. Mathematical Mode of PMSM

The rotor field-oriented control of PMSM with $i_d = 0$ is adopted to establish the dynamic mathematical model of PMSM in d - q coordinate system:

$$\begin{cases} u_d = Ri_d - \omega\psi_q + \dfrac{d\psi_d}{dt}, \\ u_q = Ri_q + \omega\psi_d + \dfrac{d\psi_q}{dt}, \end{cases} \tag{1}$$

where u_d and u_q represent the components of the d and q axis of stator voltage, respectively; i_d and i_q represent the components of the d and q axis of stator current, respectively; R represents the stator resistance; ω represents the rotor electric angular velocity; and ψ_d and ψ_q represent the components of the d and q axis of stator flux, respectively.

The stator flux linkage equation of PMSM is as follows:

$$\begin{cases} \psi_d = \psi_f + L_d i_d, \\ \psi_q = L_q i_q, \end{cases} \tag{2}$$

where ψ_f is the flux from the rotor permanent magnet turn chain to the stator winding and L_d and L_q are the inductance of the d - q axis, respectively. The electromagnetic torque equation of PMSM is as follows:

$$T_e = \frac{3}{2} p \left(\psi_d i_q - \psi_q i_d \right). \tag{3}$$

Since the motor is surface-mounted PMSM, $L_d = L_q$, substituting equation (2) into equation (3), the following equation can be obtained:

$$T_e = \frac{3}{2} p \psi_f i_q. \tag{4}$$

The motion equation of PMSM is as follows:

$$T_e - T_l - \eta\omega = J\dot{\omega}, \tag{5}$$

where T_l is the load torque of the motor, η is viscous damping, and J is the moment of inertia of the rotor. By substituting equation (4) into equation (5), the following equation can be obtained:

$$\dot{\omega} = \frac{3p}{2J} \psi_f i_q - \frac{\eta}{J} \omega - \frac{T_l}{J}. \tag{6}$$

For the multimotor system, the motion equation of the i th motor is as follows:

$$\dot{\omega}_i = \frac{3p}{2J} \psi_f i_{iq} - \frac{\eta}{J} \omega_i - \frac{T_{il}}{J}, \tag{7}$$

where i is the subscript (the same below) used to mark the variables of the ith motor. ω_i represents the speed of the i th motor, i_{iq} represents the q axis component of the stator current of the ith motor, and T_{il} represents the external load of the ith motor. Set

$$\begin{aligned} a &= \frac{3p}{2J} \psi_f, \\ u_i &= i_{iq}, \\ b &= \frac{\eta}{J}, \\ d_i &= \frac{T_{il}}{J}. \end{aligned} \tag{8}$$

Then, equation (7) can be abbreviated as

$$\dot{\omega}_i = a u_i - b\omega_i - d_i. \tag{9}$$

3. Controller Design

Based on the idea of deviation coupling control and the GFTSMC algorithm, the mean deviation coupling control strategy via global fast terminal sliding mode control is proposed. The control structure block diagram is shown in Figure 1.

Given the reference speed ω_r of each motor, there is an error between the actual speed and the given speed when the motor system starts or changes speed, which is called tracking speed error $e_{r,i}$:

$$e_{r,i} = \omega_r - \omega_i. \tag{10}$$

Under the action of the speed tracking controller, the actual speed will finally reach the given speed:

$$\lim_{t \longrightarrow +\infty} e_{r,i} = 0. \tag{11}$$

Due to the interference of the external load of each motor, the speed of the motor changes in a certain period of time, which makes the speed of each motor inconsistent. Under the multimotor synchronous control strategy proposed in this paper, the speed of a single motor is compared with the average speed, and the error between the speed of each motor and the average speed $e_{m,i}$ is obtained:

$$e_{m,i} = \omega_m - \omega_i. \tag{12}$$

The GFTSMC algorithm is used to compensate the average speed error, so that the speed of each motor is the same, and the synchronization of multimotor is realized, and the control goal is finally achieved:

$$\omega_1 = \omega_2 = \cdots\cdots = \omega_n = \omega_m = \omega_r, \tag{13}$$

where $\omega_r (i = 1, 2, \cdots, n)$ is the speed of each motor and ω_m is the average speed:

$$\omega_m = \frac{1}{n} \sum_{i=1}^{n} \omega_i. \tag{14}$$

From the above control process, it can be seen that the controller of each motor can be regarded as two subcontrollers, as shown in Figure 2. One is the speed tracking controller $C_{r,i}$, which makes the motor track the given speed signal accurately; the other is the speed compensation controller $C_{m,i}$, which compensates the difference between the motor speed and the average speed. This control structure solves the coupling problem of multimotor system. In the deviation coupling control, there is direct speed feedback between motors, which leads to the coupling problem of the multimotor system. Through the mean deviation coupling control strategy, the speed feedback obtained by the motor comes from its own speed and the average speed of all motors. The two fed back speeds form two speed differences, which are output to the current signal of a single motor through the action of the speed controller. This simplifies the

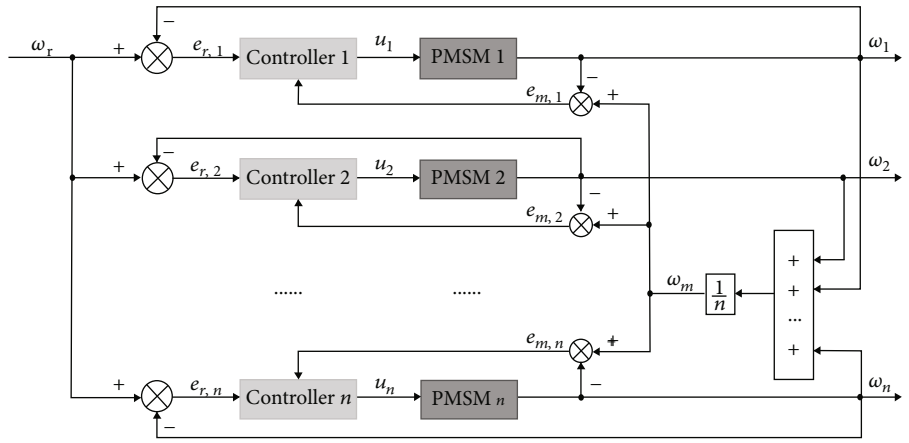

Figure 1: Mean deviation coupling control block diagram.

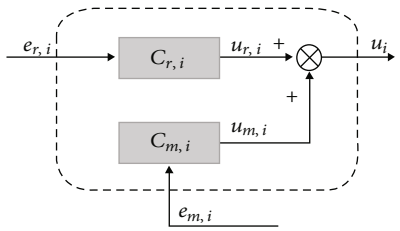

Figure 2: Structure block diagram of controller.

problem of multimotor synchronous control to the problem of single motor speed control. The coupling problem of the multimotor system is solved.

3.1. A General Method for GFTSMC Design. A high-order single-input single-output nonlinear system is considered:

$$\begin{cases} \dot{x}_m = x_{m+1}, \quad m = 1, 2, \cdots, n-1, \\ \dot{x}_n = f(x) + g(x)u, \end{cases} \tag{15}$$

where $f(x)$ and $g(x)$ are smooth functions in the R^n field and $g(x) \neq 0$, $u \in R^1$. A fast sliding mode with recursive structure is represented as [38]

$$\begin{cases} s_1 = s_0 + \alpha_0 s_0 + \beta_0 s_0^{q_0/p_0}, \\ s_2 = s_1 + \alpha_1 s_1 + \beta_1 s_1^{q_1/p_1}, \\ \cdots \\ s_{n-1} = s_{n-2} + \alpha_{n-2} s_{n-2} + \beta_{n-2} s_{n-2}^{q_{n-2}/p_{n-2}}, \end{cases} \tag{16}$$

where q_j, p_j $(q_j < p_j)$ $(j = 1, 2, \cdots n-2)$, and $\alpha_j, \beta_j > 0$ are odd numbers. In order to avoid the singularity problem in the global fast terminal sliding mode, the following conditions must be satisfied [39]:

$$\frac{q_j}{p_j} > \frac{n-j-1}{n-j}. \tag{17}$$

The global fast terminal sliding mode control law is designed as follows [38]:

$$u(t) = -\frac{1}{g(x)}\left(f(x) + \sum_{k=0}^{n-2} \alpha_k s_k^{(n-k-1)} + \sum_{k=0}^{n-2} \beta_k \frac{d^{n-k-1}}{dt^{n-k-1}} s_k^{q_k/p_k} + \varphi s_{n-1} + \gamma s_{n-1}^{q/p}\right), \tag{18}$$

where $s_0 = x_1$, $\varphi, \gamma > 0$, p and q $(p > q)$ are positive odd numbers. In the control law (18), the time for the state of the system to reach the sliding surface along the sliding surface is [38]

$$t_{s_{n-1}} = \frac{p}{\varphi(p-q)} \ln \frac{\varphi(s_{n-1}(0))^{(p-q)/p} + \gamma}{\gamma}. \tag{19}$$

3.2. Design of Speed Tracking Controller. The first derivative of velocity tracking error is

$$\dot{e}_{r,i} = \dot{\omega}_r - \dot{\omega}_i = \dot{\omega}_r - a u_i + b\omega_i + d_i. \tag{20}$$

Since PMSM is a second-order single-input single-output nonlinear control system, according to equation (15), the system state variable of the speed tracking controller $C_{r,i}$ can be set as

$$\begin{cases} x_{i1} = \int_0^t e_{r,i}(\tau) d\tau, \\ x_{i2} = e_{r,i}. \end{cases} \tag{21}$$

The global fast terminal sliding surface of the speed tracking controller is defined as

$$s_i = e_{r,i} + \alpha \int_0^t e_{r,i}(\tau) d\tau + \beta \left(\int_0^t e_{r,i}(\tau) d\tau\right)^{q/p}, \tag{22}$$

where $\alpha, \beta > 0$ and p and q $(p > q)$ are positive odd numbers. In order to avoid the singularity problem, according to equation (10), when $n = 2$ and $j = 0$, p and q should satisfy the

following conditions:

$$q < p < 2q. \tag{23}$$

The speed tracking controller is designed as follows:

$$u_{r,i} = \frac{1}{a}\left[\dot{\omega}_r + b\omega_i + d_i + ae_{r,i} + \frac{\beta d\left(\int_0^t e_{r,i}(\tau)d\tau\right)^{q/p}}{dt} + \varphi s_i + \gamma s_i^{q/p}\right]. \tag{24}$$

3.3. Design of Speed Compensation Controller. The first derivative of average velocity error is as follows:

$$\begin{aligned}\dot{e}_{m,i} &= \frac{1}{n}\sum_{j=1}^{n}\dot{\omega}_j - \dot{\omega}_i = \frac{1}{n}\sum_{j=1}^{n}\left(au_{r,j} - b\omega_j - d_j\right) - \left(au_{r,i} - b\omega_i - d_i\right)\\ &= a\left(\frac{1}{n}\sum_{j=1}^{n}u_{r,j} - u_{r,i}\right) - b\left(\frac{1}{n}\sum_{j=1}^{n}\omega_j - \omega_i\right) - \left(\frac{1}{n}\sum_{j=1}^{n}d_j - d_i\right)\\ &= a\left(\frac{1}{n}\sum_{j=1}^{n}u_{r,j} - u_{r,i}\right) - be_{m,i} - \left(\frac{1}{n}\sum_{j=1}^{n}d_j - d_i\right).\end{aligned} \tag{25}$$

The speed compensation controller is defined as

$$u_{m,i} = \frac{1}{n}\sum_{j=1}^{n}u_{r,j} - u_{r,i}. \tag{26}$$

Equation (25) can be simplified as

$$\dot{e}_{m,i} = au_{m,i} - be_{m,i} - \left(\frac{1}{n}\sum_{j=1}^{n}d_j - d_i\right). \tag{27}$$

The system state variables of speed compensation controller $C_{m,i}$ are set as follows:

$$\begin{cases} y_{i1} = \int_0^t e_{m,i}(\tau)d\tau, \\ y_{i2} = e_{m,i}. \end{cases} \tag{28}$$

The global fast terminal sliding mode surface of the speed compensation controller is expressed as follows:

$$\delta_i = e_{m,i} + \alpha\int_0^t e_{m,i}(\tau)d\tau + \beta\left(\int_0^t e_{m,i}(\tau)d\tau\right)^{q/p}. \tag{29}$$

The speed compensation controller is designed as follows:

$$u_{m,i} = \frac{1}{a}\left[be_{m,i} + \frac{1}{n}\sum_{j=1}^{n}d_j - d_i - \alpha e_{m,i} - \frac{\beta d\left(\int_0^t e_{m,i}(\tau)d\tau\right)^{q/p}}{dt} - \varphi\delta_i - \gamma\delta_i^{q/p}\right]. \tag{30}$$

3.4. Design of Load Torque Luenberger Observer. In the actual motor control system, the speed is measurable, but the load torque T_{il} is not so T_{il} and d_i are unknown. In the design of motor controller, one of them includes d_i. Therefore, it is necessary to design a load torque observer to feed back the observed values of T_{il} and d_i to the speed controller.

The state variable, input, and output of load torque Luenberger observer are selected as follows:

$$\begin{aligned}\mathbf{x} &= \begin{bmatrix}\omega_i \\ T_{il}\end{bmatrix},\\ u_i &= T_e,\\ y &= \omega_i\end{aligned} \tag{31}$$

The general form of state space variables is as follows:

$$\begin{aligned}\dot{\mathbf{x}} &= \mathbf{A}x + \mathbf{B}u_i,\\ y &= \mathbf{C}x + \mathbf{D}u_i,\end{aligned} \tag{32}$$

where **A**, **B**, **C**, and **D** are coefficient matrices, which depend on the parameters of PMSM. In this paper, when the control frequency is very high and the sampling period is very small, the load torque is a constant value in a sampling period. By changing equation (32) to the state space expression, it can be obtained that

$$\begin{aligned}\begin{bmatrix}\dot{\omega}_i \\ \dot{T}_{il}\end{bmatrix} &= \begin{bmatrix}\frac{-\eta}{J} & \frac{-1}{J} \\ 0 & 0\end{bmatrix}\begin{bmatrix}\omega_i \\ T_{il}\end{bmatrix} + \begin{bmatrix}\frac{1}{J} \\ 0\end{bmatrix}T_{ie},\\ y &= \begin{bmatrix}1\ 0\end{bmatrix}\begin{bmatrix}\omega_i \\ T_{il}\end{bmatrix}.\end{aligned} \tag{33}$$

The load torque Luenberger observer is designed as follows:

$$\begin{cases}\dot{\hat{\mathbf{x}}} = \mathbf{A}\hat{x} + \mathbf{B}u_i + \mathbf{L}(y - \hat{y}), \\ \hat{y} = \mathbf{C}\hat{x}, \end{cases} \tag{34}$$

where **L** is a coefficient matrix and

$$\begin{aligned}\mathbf{L} &= \begin{bmatrix}L_1 \\ L_2\end{bmatrix},\\ \mathbf{A} &= \begin{bmatrix}\frac{-\eta}{J} - L_1 & \frac{-1}{J} \\ -L_2 & 0\end{bmatrix},\\ \mathbf{B} &= \begin{bmatrix}\frac{1}{J} \\ 0\end{bmatrix},\\ \mathbf{C} &= \begin{bmatrix}1 & 0\end{bmatrix}.\end{aligned} \tag{35}$$

Equation (34) is derived as follows:

$$\dot{\hat{\mathbf{x}}} = (\mathbf{A}\text{-}\mathbf{LC})\hat{\mathbf{x}} + \mathbf{B}u_i + \mathbf{L}y. \tag{36}$$

Substituting equations (31) and (35) into equation (36), the following results can be obtained:

$$\begin{bmatrix} \dot{\hat{\omega}}_i \\ \dot{\hat{T}}_{il} \end{bmatrix} = \begin{bmatrix} \dfrac{-\eta}{J} - L_1 & \dfrac{-1}{J} \\ -L_2 & 0 \end{bmatrix} \begin{bmatrix} \hat{\omega}_i \\ \hat{T}_{il} \end{bmatrix} + \begin{bmatrix} \dfrac{1}{J} \\ 0 \end{bmatrix} T_{ie} + \begin{bmatrix} L_1 \\ L_2 \end{bmatrix} \omega_i. \tag{37}$$

Equation (37) is simplified as following:

$$\begin{cases} \dot{\hat{\omega}}_i = \dfrac{1}{J}\left(T_{ie} - \hat{T}_{il} - \eta\hat{\omega}_i + JL_1(\omega_i - \hat{\omega}_i)\right) \\ \dot{\hat{T}}_{il} = L_2(\omega_i - \hat{\omega}_i) \end{cases} \tag{38}$$

To make the observed load torque approach the real value, another constraint is that the eigenvalue of the **A** - **L C** matrix is less than 0 [40]. The eigenvalues of the **A**-**LC** matrix are obtained:

$$\left| \lambda\mathbf{I} - \begin{bmatrix} \dfrac{-\eta}{J} - L_1 & \dfrac{-1}{J} \\ -L_2 & 0 \end{bmatrix} \right| = 0, \tag{39}$$

where **I** is the unit matrix. Equation (39) is converted into the following form:

$$\lambda^2 + \left(\frac{\eta}{J} + L_1\right)\lambda - \frac{L_2}{J} = 0. \tag{40}$$

Set the value of the eigenvalue λ as $a1, a2$ $(a1 < 0, a2 < 0)$, and the following result can be obtained:

$$\lambda^2 - (a_1 + a_2)\lambda + a_1 a_2 = 0. \tag{41}$$

By comparing equations (40) and (41), the following equation can be obtained:

$$\begin{cases} L_1 = -\left(a_1 + a_2 + \dfrac{\eta}{J}\right), \\ L_2 = -(a_1 a_2 J). \end{cases} \tag{42}$$

By changing the values of a_1 and a_2, the speed of the observed load torque value approaching the real value is adjusted. After the load torque observed values of each motor is obtained, the observed values of d_i can be obtained as follows:

$$\hat{d}_i = \frac{\hat{T}_{il}}{J}. \tag{43}$$

Substitute $\hat{d}_i$ for d_i in equations (24) and (30) to obtain

$$u_{r,i} = \frac{1}{a}\left[\dot{\omega}_r + b\omega_i + \hat{d}_i + ae_{r,i} + \frac{\beta d\left(\int_0^t e_{r,i}(\tau)d\tau\right)^{q/p}}{dt} + \varphi s_i + \gamma s_i^{q/p}\right],$$

$$u_{m,i} = \frac{1}{a}\left[be_{m,i} + \frac{1}{n}\sum_{j=1}^{n}\hat{d}_j - \hat{d}_i - \alpha e_{m,i} - \frac{\beta d\left(\int_0^t e_{m,i}(\tau)d\tau\right)^{q/p}}{dt} - \varphi\delta_i - \gamma\delta_i^{q/p}\right]. \tag{44}$$

4. Stability Analysis

Consider a Lyapunov function:

$$V = \frac{1}{2}\sum_{i=1}^{n} s_i^2 + \frac{1}{2}\sum_{i=1}^{n}\delta_i^2. \tag{45}$$

The first derivative of V is obtained:

$$\dot{V} = \sum_{i=1}^{n} s_i\dot{s}_i + \sum_{i=1}^{n}\delta_i\dot{\delta}_i. \tag{46}$$

The first-order differential of s_i is obtained:

$$\dot{s}_i = \dot{e}_{r,i} + \alpha e_{r,i}(t) + \beta\frac{d\left(\int_0^t e_{r,i}(\tau)d\tau\right)^{q/p}}{dt}. \tag{47}$$

Substituting equation (20) into equation (47), it can be obtained that

$$\dot{s}_i = \dot{\omega}_r - au_{r,i} + b\omega_i + d_i + \alpha e_{r,i}(t) + \beta\frac{d\left(\int_0^t e_{r,i}(\tau)d\tau\right)^{q/p}}{dt}. \tag{48}$$

Substituting equation (24) into equation (48), it can be obtained that

$$\dot{s}_i = -\varphi s_i - \gamma s_i^{q/p}, \tag{49}$$

$$s_i\dot{s}_i = -\varphi s_i^2 - \gamma s_i^{(p+q)/p}. \tag{50}$$

The first derivative of δ_i is obtained:

$$\dot{\delta}_i = \dot{e}_{m,i} + \alpha e_{m,i}(t) + \frac{\beta d\left(\int_0^t e_{m,i}(\tau)d\tau\right)^{q/p}}{dt}. \tag{51}$$

Substituting equation (27) into equation (51), it can be obtained that

$$\dot{\delta}_i = au_{m,i} - be_{m,i} - \left(\frac{1}{n}\sum_{j=1}^{n} d_j - d_i\right) + \alpha e_{m,i}(t) + \frac{\beta d\left(\int_0^t e_{m,i}(\tau)d\tau\right)^{q/p}}{dt}. \tag{52}$$

Substituting equation (30) into equation (52), the following equation can be obtained:

$$\dot{\delta}_i = -\varphi\delta_i - \gamma\delta_i^{q/p}, \tag{53}$$

$$\delta_i\dot{\delta}_i = -\varphi\delta_i^2 - \gamma\delta_i^{(p+q)/p}. \tag{54}$$

Substituting equations (50) and (54) into (46), the following equation can be obtained:

$$\begin{aligned}\dot{V} = \sum_{i=1}^{n} s_i\dot{s}_i + \sum_{i=1}^{n}\delta_i\dot{\delta}_i = \sum_{i=1}^{n}\left(-\varphi s_i^2 - \gamma s_i^{(p+q)/p}\right)\\ + \sum_{i=1}^{n}\left(-\varphi\delta_i^2 - \gamma\delta_i^{(p+q)/p}\right).\end{aligned} \tag{55}$$

Since p and q are positive odd numbers and $(p+q)$ are even numbers, the following result can be obtained:

$$\begin{aligned}s_i^{(p+q)/p} &\geq 0,\\ \delta_i^{(p+q)/p} &\geq 0.\end{aligned} \tag{56}$$

It can be obtained that $\dot{V} \leq 0$. According to the Lyapunov stability theorem, the controller is asymptotically stable.

5. Experiments

In order to verify the effectiveness of the control strategy proposed in this paper, a multimotor experimental platform is built, which is composed of four permanent magnet synchronous motors with the same parameters. The experimental platform is shown in Figure 3. The work process of the experimental platform is as follows: (1) edit instruction data; (2) the upper computer software imports instruction data; (3) the upper computer sends the instruction data to each motor controller through an RS-485 multifunction converter; (4) the controller performs control according to the received instruction; and (5) the data acquisition card EM9636 collects the speed and torque signals and processes them through LabVIEW software, and then, the data are recorded. The parameters of the motor are shown in Table 1. The control structure of a single motor using the control strategy proposed in this paper is shown in Figure 4.

In the experiment, the master-slave control (MSC) strategy (motor 1 is the master motor), ring coupling control (RCC) strategy, adjacent crosscoupling control (ACCC) strategy, and mean deviation coupling control (MDCC) strategy are compared. In order to simulate the variety of load changes in the actual situation, two kinds of load forms are given to the multimotor system in the experiment:

(1) Alternate loading of each motor after no-load start

(2) Step change or continuous change of load after starting under unbalanced load

5.1. Alternate Loading of Each Motor after No-Load Start. After the motor reaches the given speed $\omega_r = 600$ r/min, load motor 1 with 10 N·m at 1 s and remove the load at 2 s; load motor 2 with 20 N·m at 3 s and remove the load at 4 s; load motor 3 with 30 N·m at 5 s and remove the load at 6 s; and load motor 4 with 40 N·m at 7 s and remove the load at 8 s. Table 2 shows the load size and time period of each motor.

Figure 5 shows the motor speed curves of the four control strategies. The orange curve represents the speed curve of motor 1, the green curve represents the speed curve of motor 2, the blue curve represents the speed curve of motor 3, and the red curve represents the speed curve of motor 4. It can be seen from the Figure 5 that when the load changes suddenly, the motor speed will fluctuate. Under the action of the controller, it will reach the steady state again after a period of time. Among the four control strategies, the speed fluctuation of the MSC is the largest, and the speed fluctuation reaches 138 r/min when the motor 4 is suddenly loaded at 7 s; under the same condition, the speed fluctuation of the MDCC is only 55 r/min, which is the smallest of the four control strategies, and its adjustment time is also the shortest. From the speed curve distribution of the four motors, the speed curve distribution of the MSC is the most discrete. The RCC and the ACCC are better than the MSC; however, they are all worse than the MDCC.

In order to evaluate the synchronization performance of each control strategy more intuitively, two kinds of statistics are used to describe the synchronization degree of each control strategy:

(1) Range

$$\text{Range} = \max(\omega_i) - \min(\omega_i), \quad (i = 1, 2, 3, 4) \tag{57}$$

(2) Mean deviation (MD)

$$\text{MD} = \frac{1}{4}\sum_{i=1}^{4}|\omega_i - \omega_m| \tag{58}$$

Figure 6 shows the range curves of the four control strategies. The orange curve represents the MSC, the green curve represents the ACCC, the blue curve represents the RCC, and the red curve represents the MDCC. It can be seen from Figure 6 that when the load increases suddenly, with the increase of the load value, the range of the four control strategies become larger. When loading motor 1, since motor 1 of the MSC is the master motor, the range value of the MSC at 1 s is not the largest. When the load is suddenly increased on the slave motor, the range of MSC is the largest. The range of the four control strategies at the moment of sudden load is shown in Table 3.

It can be seen from Table 3 that when motor 1 load changes suddenly, the range of the RCC is the largest, reaching 18.0 r/min and 18.1 r/min, and the range of the MDCC is the smallest, being 8.0 r/min and 7.7 r/min, respectively. When motor 2 load changes suddenly, the range of the MSC is the largest, reaching 66.7 r/min and 67.0 r/min. The

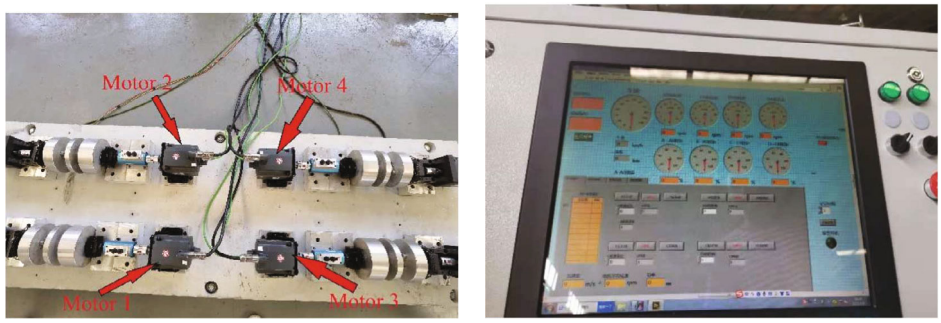

(a) (b)

Figure 3: Four-motor experimental platform: (a) four-motor platform; (b) control platform.

Table 1: Parameters of PMSM.

Symbol	Quantity	Value
Ψ_f	Rotor magnetic flux	0.175 Wb
L_d	Inductance of d axis	0.835 mH
L_q	Inductance of q axis	0.835 mH
R	Stator resistance	2.875 Ω
J	Rotor inertia	0.003 kg·m^2
B	Viscous friction coefficient	0.008 N·m·s
p	Number of pole pairs	4

range of the RCC is 36.4 r/min, and the range of the ACCC is 36.4 r/min. The range is 26.0 r/min and 26.1 r/min, and the range of the MDCC is the smallest, which is 16.8 r/min and 16.5 r/min. When motor 3 load changes suddenly, the range value of the MSC is the largest, which is 101.5 r/min and 101.9 r/min, followed by the RCC, which is 54.7 r/min and 55.1 r/min. The range of the ACCC is 39.3 r/min and 38.6 r/min, and the range of the MDCC is 25.6 r/min and 25.9 r/min. When the load of motor 4 changes suddenly, the range of MSC is still the largest, 137.4 r/min and 136.9 r/min; the range of ACCC is 51.6 r/min and 51.3 r/min; the range of RCC is 73.1 r/min and 73.3 r/min; and the range of MDCC is the smallest, 34.9 r/min and 33.9 r/min.

Figure 7 shows the mean deviation curves of the four control strategies. The orange curve represents the MSC, the green curve represents the ACCC, the blue curve represents the RCC, and the red curve represents the MDCC. It can be seen from Figure 7 that when the load changes suddenly, the mean deviation of each control strategy increases with the increase of the load value. When the load of motor 1 changes suddenly, the RCC has the largest mean deviation, which is 5.9 r/min and 5.8 r/min; the ACCC has the mean deviation of 4.3 r/min and 4.2 r/min; the MSC has the mean deviation of 3.7 r/min and 3.4 r/min; and the MDCC has the smallest mean deviation, which is 3.0 r/min and 2.9 r/min. When the load of motor 2 changes suddenly, the mean deviation of the MSC is the largest, being 25.1 r/min and 25.2 r/min, followed by the mean deviation of the RCC, 11.8 r/min, and the mean deviation of ACCC is 8.5 r/min and 8.4 r/min; the mean deviation of the MDCC is the smallest, which is 6.3 r/min and 6.2 r/min. When the load of motor 3 changes suddenly, the mean deviation of the MSC is still the largest, which is 38.0 r/min and 38.1 r/min, followed by the mean deviation of the RCC, which is 17.6 r/min and 17.8 r/min. The mean deviation of the ACCC is 12.7 r/min and 12.6 r/min, and the mean deviation of the MDCC is the smallest, which is 9.5 r/min and 9.6 r/min. When the load of motor 4 changes suddenly, the mean deviation of MSC is the largest, which is 68.6 r/min and 68.4 r/min, about three times of the mean deviation of RCC; the mean deviation of ACCC is 16.8 r/min and 16.9 r/min; and the mean deviation of MDCC is the smallest, which is 13.0 r/min and 12.6 r/min. Table 4 shows the mean deviation of the four control strategies when the motor load changes suddenly.

It can be seen from the data that no matter the range or the average difference, under the same load conditions, the four-motor system adopting the MDCC can get the minimum range and mean deviation, and it can be seen from Figures 6 and 7 that the range and mean deviation of the MDCC converge faster than the other three strategies. The experimental results show that under the condition of single motor loading successively, the speed synchronization degree of multimotor system with MDCC is better.

Figure 8 shows the curve of the real value of the load torque and the observed value obtained by the Luenberger observer. In Figure 8, the red curve represents the real value of load torque, and the blue curve represents the observed value. It can be seen from the figure that the observed value of load torque can better track the real value. Only when the load changes suddenly, there is an error between the observed value and the real value, and the error will converge to zero quickly.

5.2. Step Change or Continuous Change of Load after Starting under Unbalanced Load. The given speed of each motor is $\omega_r = 600$ r/min, where motor 1 and motor 2 start with no load, motor 3 starts with a load of 10 N·m, and motor 4 starts with a load of 30 N·m. After reaching the given speed, motor 1 loads 10 N·m at 1.5 s, until 3 s, the load increases to 30 N·m, and the load drops to 0 at 4 s; motor 2 has a sudden load increase of 30 N·m at 2 s, then a sudden load drop of 10 N·m at 3.5 s, and then a sudden drop to 0 at 4.5 s; motor 3 started under a load of 10 N·m, and then, from 2.5 s, the load torque suddenly dropped to 0 when the speed increased

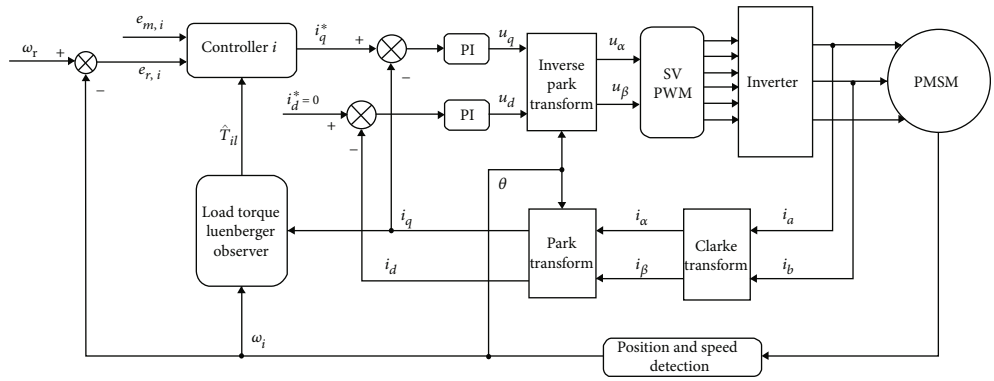

Figure 4: Structure block diagram of single motor system.

Table 2: Load size and time period of each motor (N·m).

	0—1 s	1—2 s	2—3 s	3—4 s	4—5 s	5—6 s	6—7 s	7—8 s
Motor 1	0	10	0	0	0	0	0	0
Motor 2	0	0	0	20	0	0	0	0
Motor 3	0	0	0	0	0	30	0	0
Motor 4	0	0	0	0	0	0	0	40

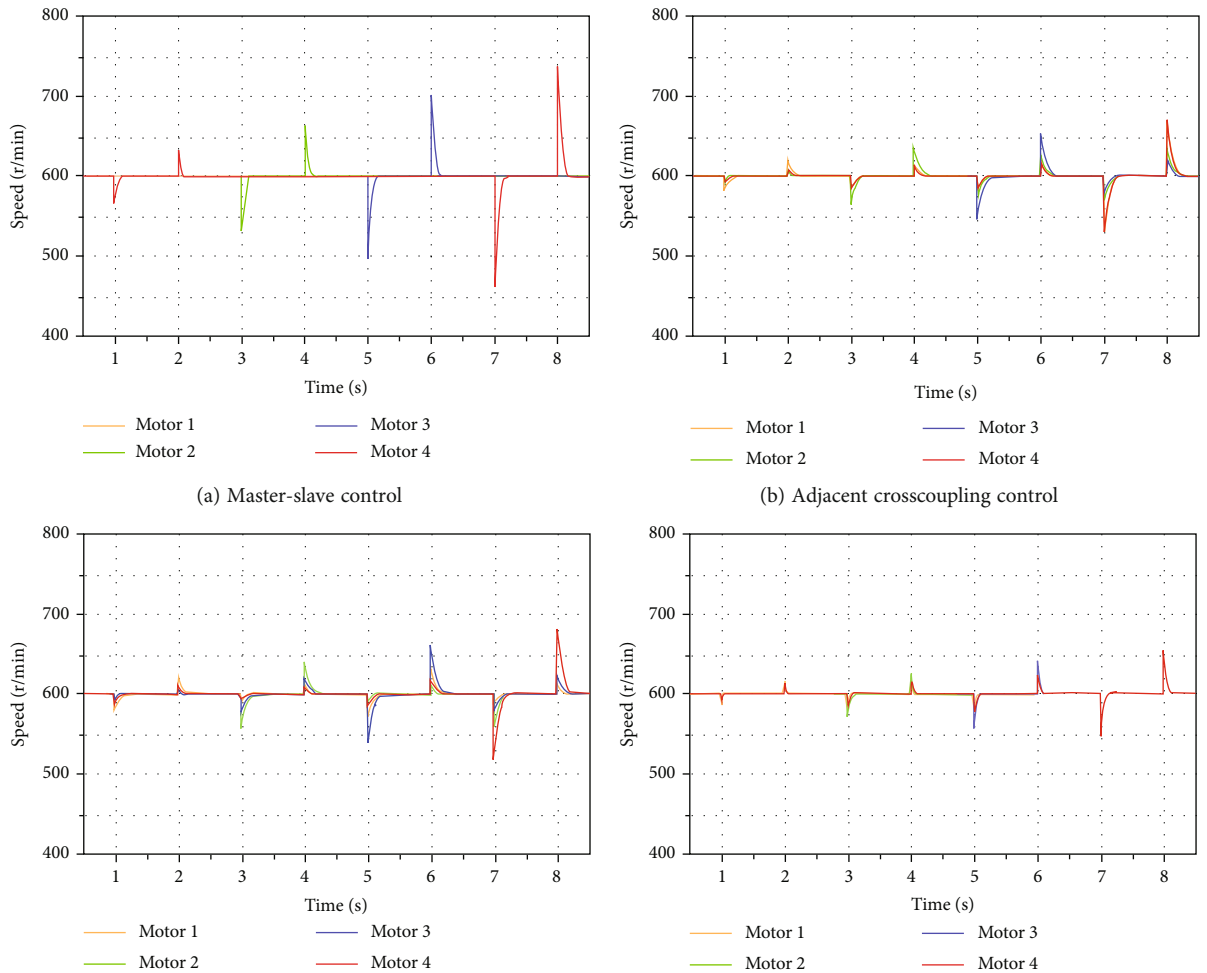

(a) Master-slave control

(b) Adjacent crosscoupling control

(c) Ring coupling control

(d) Mean deviation coupling control

Figure 5: Motor speed curves of the four control strategies.

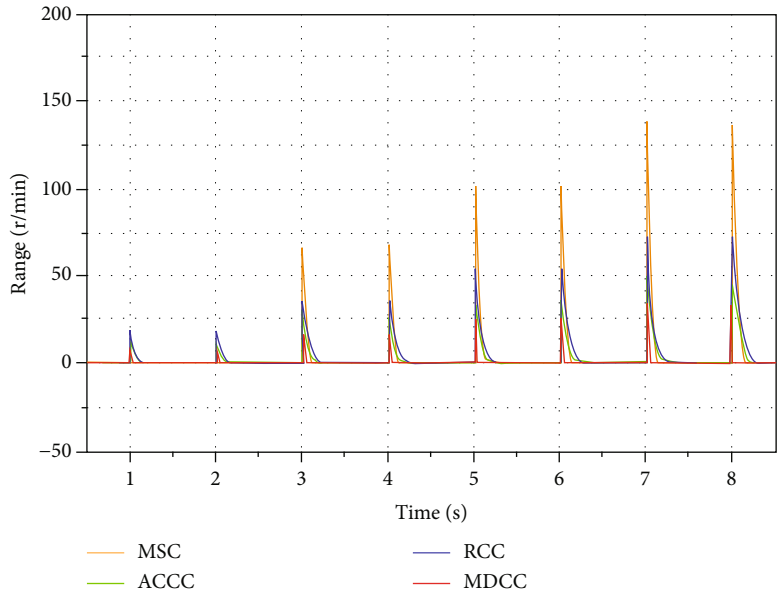

Figure 6: The range curves of four motors for the four control strategies.

Table 3: The range of the four control strategies at the moment of the motor load changes suddenly (r/min).

	1 s	2 s	3 s	4 s	5 s	6 s	7 s	8 s
MSC	15.0	13.7	66.7	67.0	101.5	101.9	137.4	136.9
ACCC	13.5	13.0	26.0	26.1	39.3	38.6	51.6	51.3
RCC	18.0	18.1	36.4	36.4	54.7	55.1	73.1	73.3
MDCC	8.0	7.7	16.8	16.5	25.6	25.9	34.9	33.9

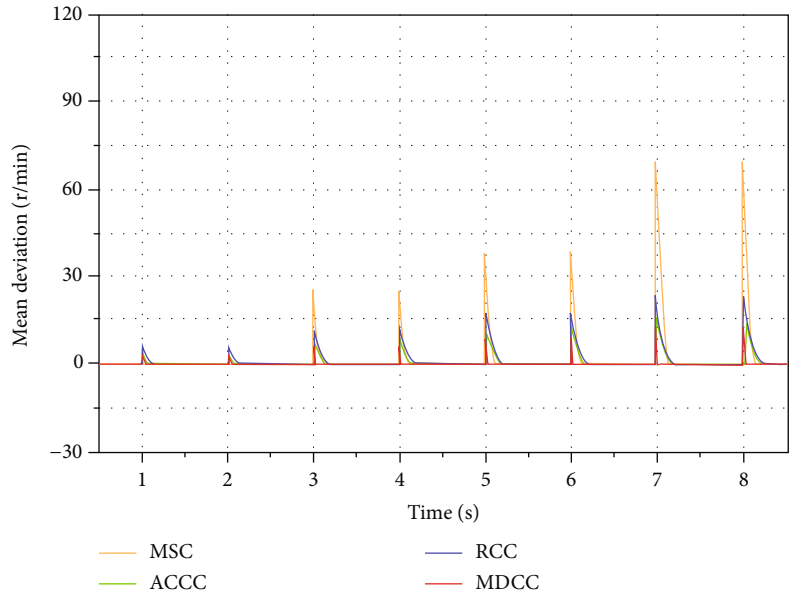

Figure 7: The mean deviation curves of the four control strategies.

to 5 s at a speed of 4 t; motor 4 was started under a load of 30 N·m, and then, from 2.5 s, the load torque suddenly dropped to 0 when the speed decreases to 5 s at a speed of 6 t. Table 5 shows the load of each motor in each time period.

Figure 9 shows the motor speed curves of each control strategy under this kind of load. The orange curve, green curve, blue curve, and red curve represent the speed of motor 1, motor 2, motor 3, and motor 4, respectively.

Table 4: The mean deviation of four control strategy when the motor load changes suddenly (r/min).

	1 s	2 s	3 s	4 s	5 s	6 s	7 s	8 s
MSC	3.7	3.4	25.1	25.2	38.0	38.1	68.6	68.4
ACCC	4.3	4.2	8.5	8.4	12.7	12.6	16.9	16.8
RCC	5.9	5.8	11.8	11.8	17.6	17.8	23.7	23.7
MDCC	3.0	2.9	6.3	6.2	9.5	9.6	13.0	12.6

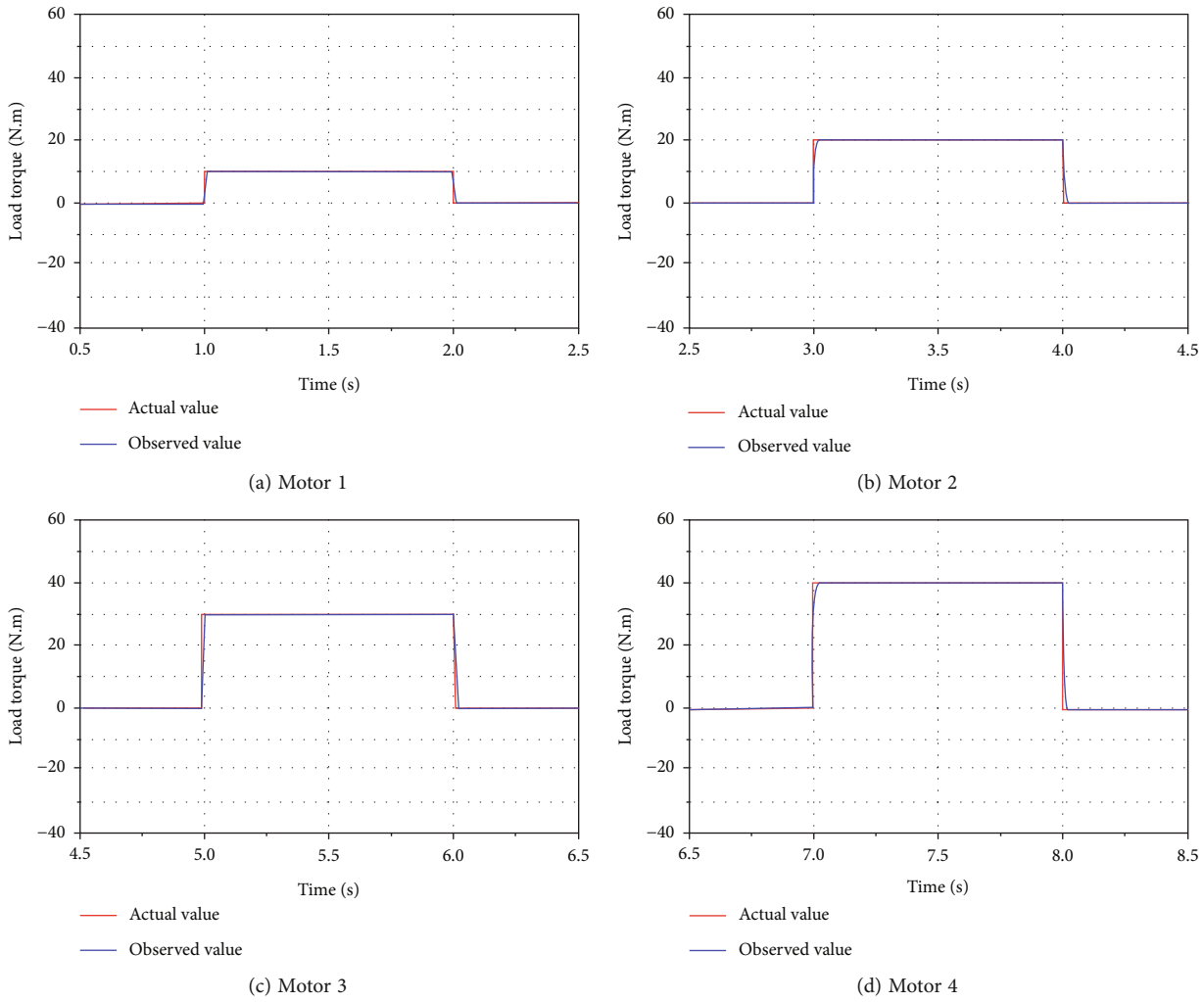

Figure 8: The curve of actual value and observed value of load torque.

It can be seen from Figure 9 that the speed fluctuation of the motor is the biggest at the two moments when the load changes the most. The speed fluctuation of the four-motor system adopting the MSC reaches 100 r/min at these two moments, while the speed fluctuation of the four-motor system adopting the MDCC is 38 r/min at these two moments, and the speed fluctuation values of the four-motor system adopting ACCC and RCC are between them, which are 52 r/min and 59 r/min, respectively. Figure 9 also shows that the controller can better regulate the speed of the motor to keep it in a steady state during the period of gradual load change of the motor.

Figure 10 shows the range curve of the four control strategies under the second load form. Due to unbalanced starting, there will be speed difference when the motor starts to a stable state. It can be seen from Figure 10 that the range of the MSC at startup is the largest, reaching 110.2 r/min, followed by the range of the RCC, 49.7 r/min, and the range of ACCC is 29.1 r/min. The range of the MDCC is the smallest, which is 24.4 r/min. At 1.5 s, when the load of motor 1 suddenly increases by 10 N·m, the range of the MSC, ACCC, RCC, and MDCC is 15.0 r/min, 13 r/min, 18.5 r/min, and 8.1 r/min, respectively. At 2 s, when the load of motor 2 increased by 30 N·m, the range of the MSC is the largest, which is 102.7 r/min, followed

Table 5: The load of each motor in each time period (N·m).

	0—1.5 s	1.5—2 s	2—2.5 s	2.5—3 s	3—3.5 s	3.5—4 s	4—4.5 s	4.5—5 s	5—6 s
Motor 1	0		10		30			0	
Motor 2		0		30		10		0	
Motor 3		10				$4t$			0
Motor 4		30				$-6t+45$			0

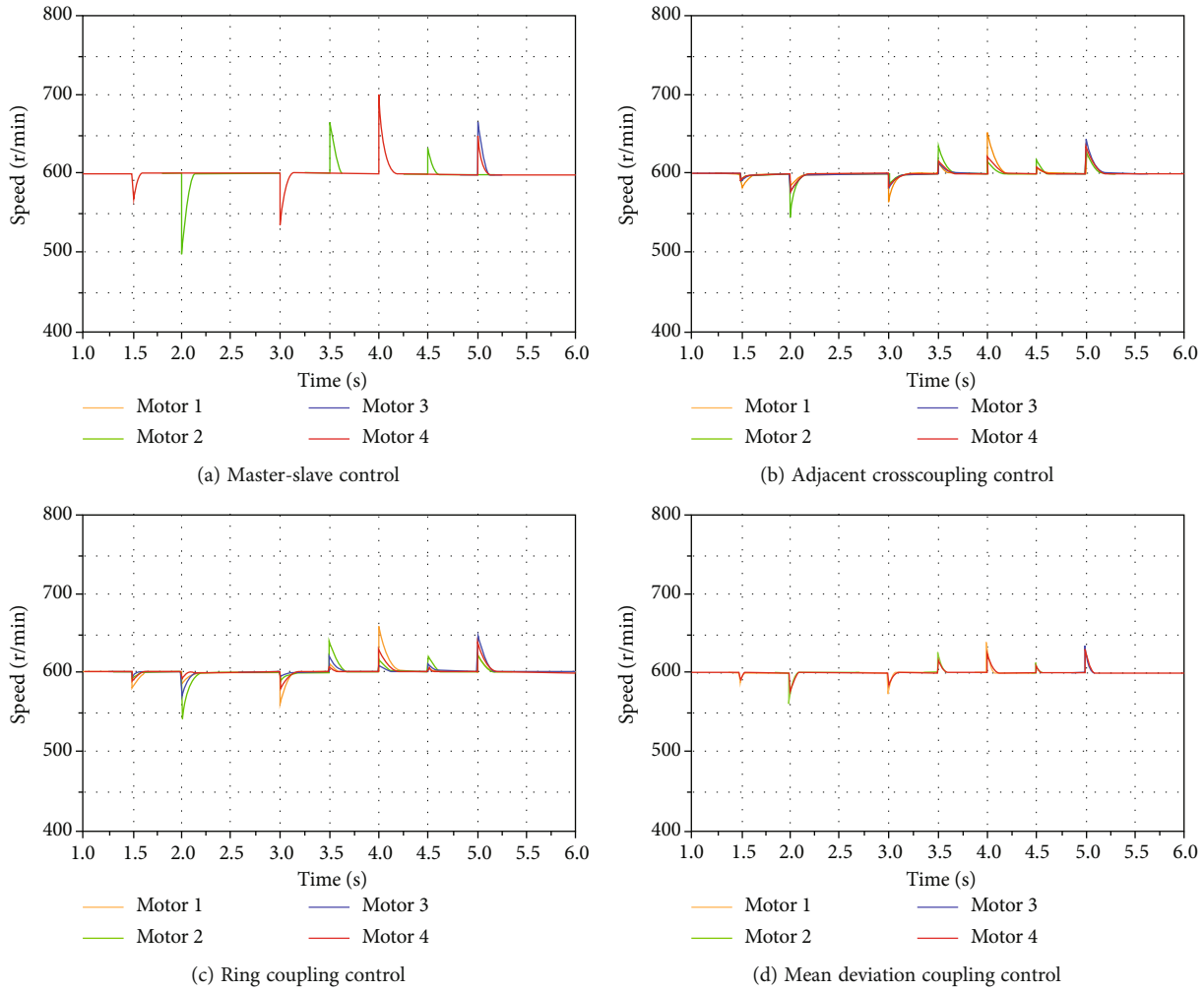

(a) Master-slave control

(b) Adjacent crosscoupling control

(c) Ring coupling control

(d) Mean deviation coupling control

Figure 9: Motor speed curves of the four control strategies.

by the range of the RCC, which is 55.0 r/min. The range of the ACCC is 38.7 r/min, and the range of the MDCC is the smallest, which is 25.7 r/min. At 3 s, when the load of motor 1 increases from 10 N·m to 30 N·m, the range of the RCC is the largest, which is 36.5 r/min, and the range of the MSC is 28.8 r/min, the range of the ACCC is 26.3 r/min, and the range of the MDCC is the smallest, which is 17.5 r/min. At 3.5 s, the load of motor 2 dropped from 30 N·m to 10 N·m. At this moment, the range of the MSC is the largest, which is 67.9 r/min, and the range of the RCC is 36.6 r/min, the range of the ACCC is 26.2 r/min, and the range of the MDCC is 16.6 r/min. At 4 s, when the load of motor 1 suddenly drops from 30 N·m to 0, the range of the RCC is the largest at 54.6 r/min, and the range of the MSC is 45.4 r/min. The range of the ACCC is 39.0 r/min, and the range of the MDCC is the smallest, which is 25.3 r/min. At 4.5 s, when the load of motor 2 drops suddenly from 10 N·m to 0, the range of MSC, ACCC, RCC, and MDCC is 35.5 r/min, 13.0 r/min, 18.0 r/min, and 8.3 r/min, respectively. At 5 s, the load of motor 3 dropped from 20 N·m to 0, and the load of motor 4 dropped from 15 N·m to 0. At this moment, the range of the MSC is the largest, which is 67.7 r/min. The range of the RCC is 28.0 r/min, the range of the ACCC is 17.1 r/min, and the range of the MDCC is the smallest, which is 16.9 r/min. Table 6 shows the range of the four control strategies at the moment of the motor load changes suddenly.

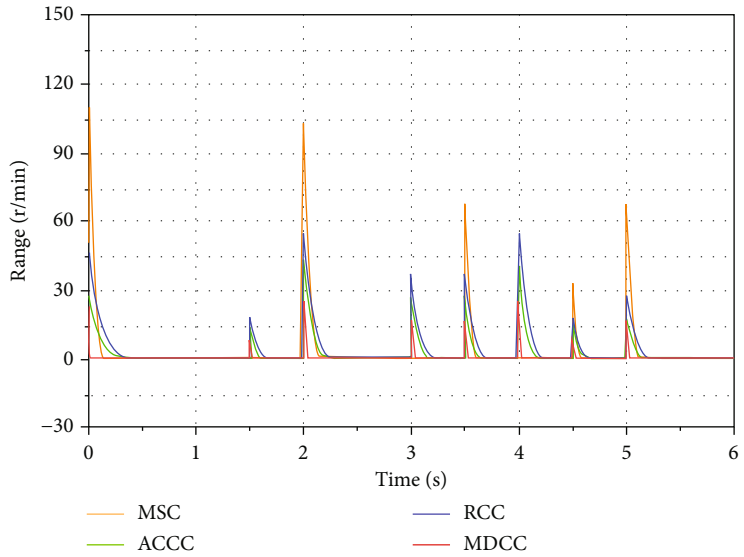

Figure 10: The range curve of the four control strategies.

Table 6: The range of four control strategy at the moment of the motor load changes suddenly (r/min).

	0 s	1.5 s	2 s	3 s	3.5 s	4 s	4.5 s	5 s
MSC	110.2	15.0	102.7	28.8	67.9	45.4	35.5	67.7
ACCC	29.1	13.0	38.7	26.3	26.2	39.0	13.0	17.1
RCC	49.7	18.5	55.0	36.5	36.6	54.6	18.0	28.0
MDCC	24.4	8.1	25.7	17.5	16.6	25.3	8.3	16.9

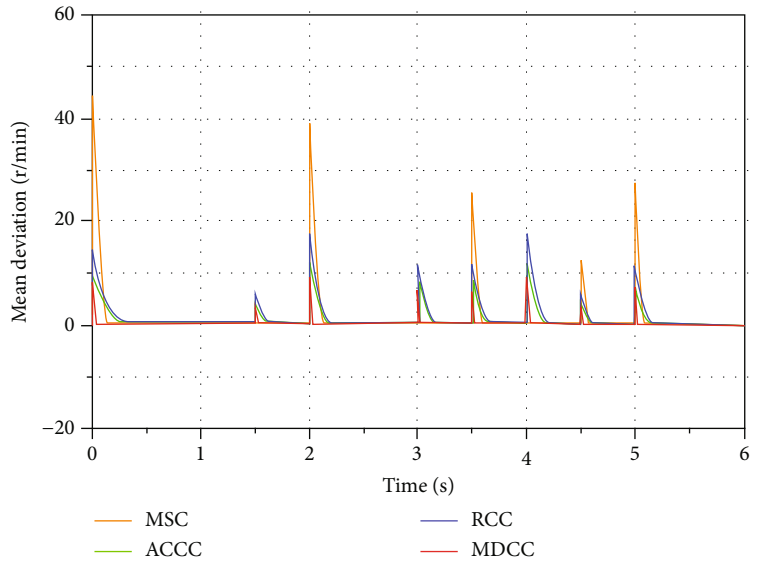

Figure 11: The mean deviation curve of the four control strategies.

Figure 11 shows the mean deviation curve of the four control strategies under the second load form. When the load of motor 1 changes suddenly, among the four control strategies, the mean deviation of the RCC is the largest; when the load of other motors changes suddenly, the mean deviation of the MSC is the largest. Table 7 shows the mean deviation of the four control strategies when the load of each motor changes suddenly under this type of load.

It can be seen from Table 7 that when there is a sudden change in the load of motor 1, the mean deviation of the RCC is the largest; the order from large to small is as follows: the mean deviation of RCC, the mean deviation of MSC, the

Table 7: The mean deviation of four control strategy at the moment of the motor load changes suddenly (r/min).

	0 s	1.5 s	2 s	3 s	3.5 s	4 s	4.5 s	5 s
MSC	43.8	3.6	38.3	7.1	25.2	11.3	12.1	27.2
ACCC	10.6	4.2	12.7	8.6	8.5	12.6	4.3	7.1
RCC	14.7	6.0	17.8	11.9	11.9	17.7	5.8	11.4
MDCC	8.1	3.0	9.5	6.5	6.2	9.4	3.1	7.0

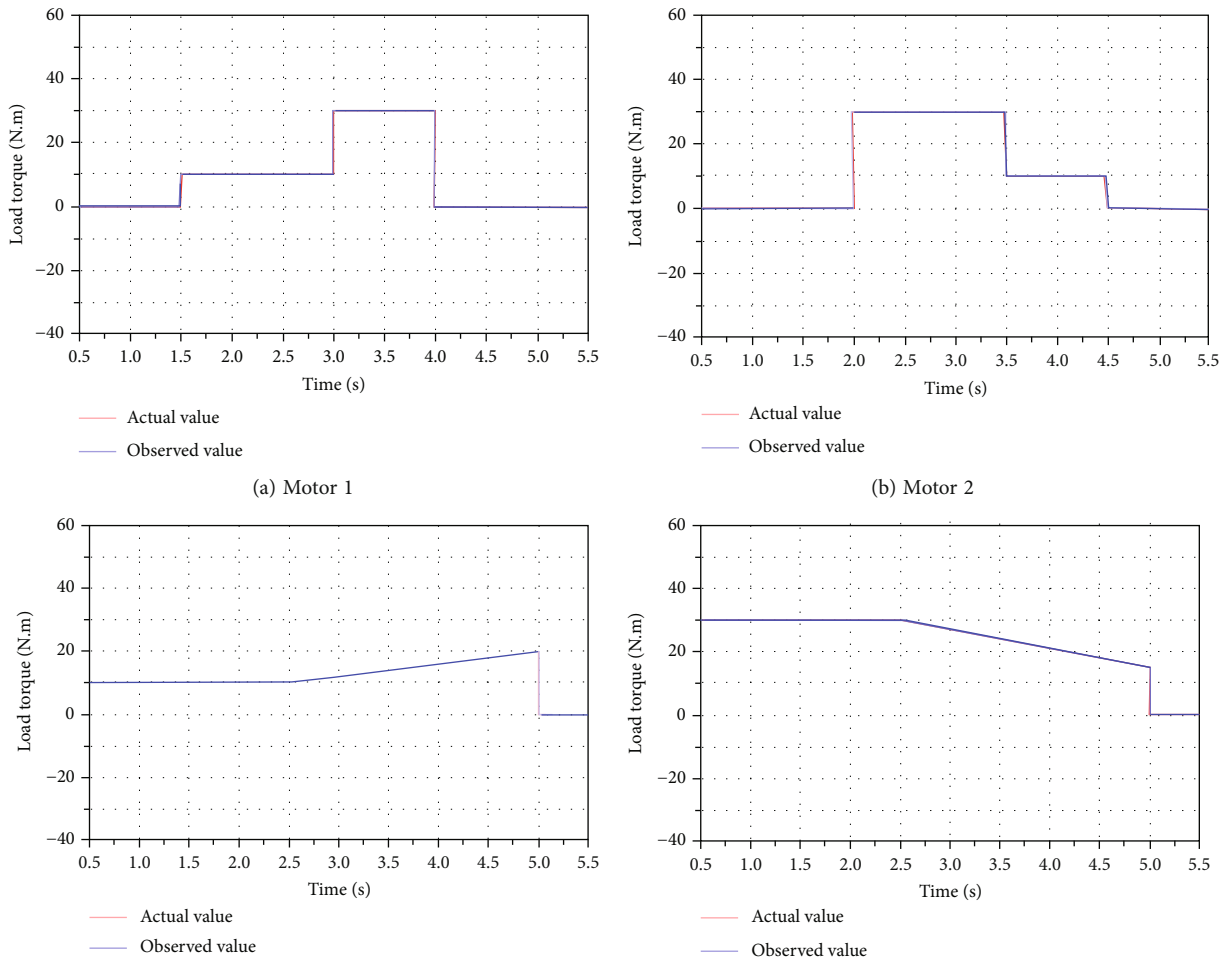

Figure 12: The curve of actual value and observed value of load torque.

mean deviation of ACCC, and the mean deviation of MDCC; when there is a sudden change in the load of the other motors, the mean deviation of the MSC is the largest, followed by the mean deviation of the RCC, the mean deviation of the MDCC is the smallest, and the mean deviation of the ACCC is between the mean deviation of RCC and the MDCC.

Tables 6 and 7 and Figures 10 and 11 show that under the second load form, the range and mean deviation of the four-motor system using MDCC are the smallest, and the time for the range and average difference to converge to 0 are the shortest. The test results show that the multimotor system using MDCC has the best degree of synchronization in the case of sudden or gradual changes in load after unbalanced startup.

Figure 12 shows the curve of the real value of the load torque and observed value obtained by the observer. It can be seen from Figure 12 that no matter the load is abrupt or gradual, the load torque Luenberger observer can better track the actual value, and the error between them can quickly converge to 0. The experimental results show that the load torque Luenberger observer is effective.

6. Conclusions

This study has successfully proved the effectiveness of the proposed mean deviation coupling control for the multimotor system via global fast terminal sliding mode control. First, the mathematical model of the PMSM is established, which provides a mathematical foundation for the controller design; secondly, combined with the global fast terminal sliding mode control algorithm, the multimotor mean deviation coupling synchronous controller is designed, and the deviation coupling control strategy is optimized. The structure reduces the calculation amount of the control system and improves the synchronization accuracy of the system. In addition, the load torque Luenberger observer is designed to observe the external load of the motor in real time and feed it back to the controller. The stability of the controller is analyzed based on the Lyapunov stability theorem, and it is concluded that the designed controller is asymptotically stable. Finally, a four-motor experimental platform was built. The experimental results show that the load torque Luenberger observer can better estimate the actual load value. By comparing with other commonly used multimotor synchronous control strategies, the result of the proposed control strategy with higher synchronization accuracy is obtained, and the effectiveness of the proposed control strategy is verified. The effectiveness of the proposed control strategy is verified.

Data Availability

The data used to support the findings of this study are available from the corresponding author upon request.

Conflicts of Interest

The authors declare that they have no known competing financial interests or personal relationships that could have appeared to influence the work reported in this paper.

Acknowledgments

This study was funded by National Key Research and Development Plan of China, grant number 2016YFC0802903.

References

[1] W. Li, "Application of PMSM control in electric vehicle," *Internal Combustion Engine & Parts*, vol. 298, no. 22, pp. 51-52, 2019.

[2] T. Shi, H. Liu, Q. Geng, and C. Xia, "Improved relative coupling control structure for multi-motor speed synchronous driving system," *IET Electric Power Applications*, vol. 10, no. 6, pp. 451–457, 2016.

[3] M. Li and X. Meng, "Analysis and design of system for multimotor synchronous control," in *CSEE 2011: Advances in Computer Science, Environment, Ecoinformatics, and Education-International Conference*, Wuhan, China, 2011 August 21-22.

[4] L. Li, L. Sun, and S. Zhang, "Mean deviation coupling synchronous control for multiple motors via second- order adaptive sliding mode control," *ISA Transactions*, vol. 62, pp. 222–235, 2016.

[5] A. Cordeiro, J. Manuel, and V. F. Pires, "Performance of synchronized master-slave closed-loop control of AC electric drives using real time motion over ethernet (RTMoE)," *Mechatronics*, vol. 69, no. 4, article 102400, 2020.

[6] W. Chen, J. Liang, and T. Shi, "Speed synchronous control of multiple permanent magnet synchronous motors based on an improved cross-coupling structure," *Energies*, vol. 11, no. 2, p. 282, 2018.

[7] C. S. Chen and L. Y. Chen, "Robust cross-coupling synchronous control by shaping position commands in multiaxes system," *IEEE Transactions on Industrial Electronics*, vol. 59, no. 12, pp. 4761–4773, 2012.

[8] K. H. Su and M. Y. Cheng, "Contouring accuracy improvement using cross-coupled control and position error compensator," *International Journal of Machine Tools & Manufacture*, vol. 48, no. 12-13, pp. 1444–1453, 2008.

[9] D. Z. Zhao, C. W. Li, and J. Ren, "Speed synchronisation of multiple induction motors with adjacent cross-coupling control," *IET Control Theory & Applications*, vol. 4, no. 1, pp. 119–128, 2010.

[10] Y. Zhang, H. Deng, and Y. Zhang, "Synchronization control of space voltage vector controlled multi-PMSM based on adjacent cross-coupling," *Advanced Materials Research*, vol. 383, pp. 6391–6397, 2012.

[11] R. Liu, J. Z. Sun, Y. Q. Luo, W. Sun, and W. D. Li, "Research on multi-motor synchronization control based on the ring coupling strategy for cutterhead driving system of shield machines," *Applied Mechanics & Materials*, vol. 52, pp. 65–72, 2011.

[12] X. Y. Peng, W. Liu, and Q. Zhang, "Synchronized control of multi-motor based on the improved relative coupling control," *Journal of Hunan University*, vol. 40, no. 11, pp. 77–83, 2013.

[13] F. Dong, J. C. Yang, T. Z. Gao et al., "The research and design of virtual spindle vibration test system," *Applied Mechanics & Materials*, vol. 556, no. 22, pp. 2903–2905, 2014.

[14] P. Liang, W. Zhou, and Z. Yang, "The multi-motor synchronous control based on fuzzy PID master-slave method," *Microcomputer & Its Applications*, vol. 35, no. 15, pp. 5–7, 2016.

[15] H. Huang, Q. Tu, C. Jiang, L. Ma, P. Li, and H. Zhang, "Dual motor drive vehicle speed synchronization and coordination control strategy," *AIP Conference Proceedings*, vol. 1955, pp. 1–9, 2018.

[16] Y. Koren, "Cross-coupled biaxial computer control for manufacturing systems," *Journal of Dynamic Systems, Measurement, and Control*, vol. 102, no. 4, pp. 265–272, 2019.

[17] L. Wang and Y. Tang, "Fuzzy cross-coupling control for dual linear motors based on preview feedforward compensation," in *International Conference on Mechatronics and Automation*, pp. 2138–2142, Changchun, China, 2009.

[18] W. Chen, D. D. Wang, Q. Geng, and C. L. Xia, "Robust adaptive cross-coupling position control of biaxial motion system," *Science China Technological Sciences*, vol. 59, no. 4, pp. 680–688, 2016.

[19] A. J. Crispin, L. Ibrani, G. E. Taylor, and G. Waterworth, "Neural network cross-coupling gain controller for a bi-axial contouring system," in *Proceedings of the 1999 American Control Conference*, pp. 351–357, San Diego, CA, USA, 1999.

[20] W. Chen, Y. Wu, R. du, Q. Chen, and X. Wu, "Speed tracking and synchronization of a dual-motor system via second order

sliding mode control," *Mathematical Problems in Engineering*, vol. 2013, 10 pages, 2013.

[21] C. Zhu, Q. Tu, C. Jiang, M. Pan, and H. Huang, "A cross coupling control strategy for dual-motor speed synchronous system based on second order global fast terminal sliding mode control," *IEEE Access*, vol. 8, pp. 217967–217976, 2020.

[22] P. Pinal, C. Nunez, R. Alvarez, and I. Cervantes, "Comparison of multi-motor synchronization techniques," in *30th Annual Conference of IEEE Industrial Electronics Society, 2004. IECON 2004*, pp. 1670–1675, Busan, Korea, 2004.

[23] P. Li, W. Wang, and Y. Wan, "Multi-motor fuzzy PID synchronous control based on the adjacent deviation coupling strategy," *Machine Design & Research*, vol. 5, no. 29, pp. 45–48, 2013.

[24] Y. B. Wang and K. Cao, "Brief introduction of multi-motor synchronous control technology," *Small & Special Electrical Machines*, vol. 8, no. 47, pp. 69–73, 2019.

[25] A. Jimenez-Fernandez, G. Jimenez-Moreno, A. Linares-Barranco, M. J. Dominguez-Morales, R. Paz-Vicente, and A. Civit-Balcells, "A neuro-inspired spike-based PID motor controller for multi-motor robots with low cost FPGAs," *Sensors*, vol. 12, no. 4, pp. 3831–3856, 2012.

[26] J. Askari, J. Soltani, G. R. Arab Markadeh, and N. R. Abjadi, "Nonlinear sliding-mode control of a multi-motor web-winding system without tension sensor," *IET Control Theory & Applications*, vol. 3, no. 4, pp. 419–427, 2009.

[27] Z. Tian, S. Li, Y. Wang, and Q. Zhang, "Multi permanent magnet synchronous motor synchronization control based on variable universe fuzzy PI method," *Engineering Letters*, vol. 23, no. 3, 2015.

[28] W. Zhao and X. Ren, "Neural network-based tracking and synchronization control for nonlinear multi-motor driving servomechanism," in *Proceedings of the 35th Chinese Control Conference*, pp. 3525–3530, Chengdu, China, 2016.

[29] P. F. Jin, Y. Xie, J. Wang, and L. J. Xiao, "Sliding mode control of permanent magnet synchronous motor based on load torque observer," *Small & Special Electrical Machines*, vol. 46, no. 8, pp. 62–64, 2018.

[30] X. G. Zhang, L. Sun, and K. Zhao, "Sliding mode control of PMSM based on a novel load torque sliding mode observer," *Proceedings of the CSEE*, vol. 32, no. 22, pp. 111–116, 2012.

[31] J. J. Slotine and S. S. Satry, "Tracking control of non-linear systems using sliding surfaces, with application to robot manipulators†," *International Journal of Control*, vol. 38, no. 2, pp. 465–492, 1983.

[32] W. B. Gao, *Theory and Design Method of Variable Structure Control*, Science Press, Beijing, 1996.

[33] Y. B. Sun, Q. D. Guo, and Y. N. Sun, "Sliding mode variable structure control of AC linear servo system based on fuzzy self-learning," *Transactions of China Electrotechnical Society*, vol. 26, no. 1, pp. 136–139, 2019.

[34] X. H. Yu and Z. H. Man, "Model reference adaptive control systems with terminal sliding modes," *International Journal of Control*, vol. 64, no. 6, pp. 1165–1176, 1996.

[35] K. Y. Zhuang, K. Q. Zhang, and H. Y. Su, "Terminal sliding mode control for higher order nonlinear systems," *Journal of Zhejiang University*, vol. 36, no. 5, pp. 482–485, 2002.

[36] Y. Feng, X. H. Yu, and Z. H. Man, "Non-singular terminal sliding mode control of rigid manipulators," *Automatica*, vol. 28, no. 12, pp. 2159–2167, 2002.

[37] J. K. Liu and F. C. A. Sun, "A novel dynamic terminal sliding mode control of uncertain nonlinear systems," *Journal of Control Theory and Applications*, vol. 5, no. 2, pp. 189–193, 2007.

[38] S. H. Yu, X. H. Yu, and Z. H. Man, "Robust global terminal sliding mode control of SISO nonlinear uncertain systems," in *Proceedings of the 39th IEEE Conference on Decision and Control*, pp. 2198–2203, Sydney, NSW, 2000.

[39] X. H. Yu and Z. H. Man, "Fast terminal sliding-mode control design for nonlinear dynamical systems," *IEEE Transactions on Circuits and Systems I: Fundamental Theory and Applications*, vol. 49, no. 2, pp. 261–264, 2002.

[40] Z. Li, G. D. Hu, J. R. Cui, and G. Y. Liu, "Sliding-mode variable structure control with integral action for permanent magnet synchronous motor," *Proceedings of the CSEE*, vol. 34, no. 2, pp. 431–437, 2014.